# Determination of thermal expansion, defect formation energy, and defect-induced strain of α-U via *ab initio* molecular dynamics

Benjamin Beeler[a,b,*], Khadija Mahbuba[a], Yuhao Wang[c], Andrea Jokisaari[b]

[a]*North Carolina State University, Raleigh, NC 27607*
[b]*Idaho National Laboratory, Idaho Falls, ID 83415*
[c]*University of Michigan, Ann Arbor, MI 48109*

## Abstract

Uranium (U) is often alloyed with molybdenum (Mo) or zirconium (Zr) in order to stabilize its high-temperature body-centered cubic phase for use in nuclear reactors. However, in all metallic fuel forms, the $\alpha$ phase of U remains in some fraction. This phase decomposition due to temperature or compositional variance can play an outsized role on fuel performance and microstructural evolution. Relatively little is known about fundamental point defect properties in $\alpha$-U at non-zero temperatures, from either computational or experimental studies. This work performs the first thorough evaluation of the $\alpha$ phase of U via *ab initio* molecular dynamics (AIMD). A number of thermophysical properties are calculated as a function of temperature, including equilibrium lattice parameters, thermal expansion, and heat capacity. These results indicate a two-region behavior, with the transition at 400 K. The thermal expansion expansion/contraction in the $a/b$ direction occurs rapidly from 100 K up to 400 K, after which a more linear and gradual change in the lattice constant takes place. The volumetric expansion matches experiments quantitatively, but the individual lattice constant expansion only matches experiments qualitatively. Point defect formation energies and induced lattice strains are also determined as a function of temperature, providing insight on defect populations and the fundamentals of irradiation growth in $\alpha$-U. Interstitials induce significantly more strain than vacancies, and the nature of that strain is highly dependent on the individual lattice directions. The direction of point defect induced lattice strain is contrary to the irradiation growth behavior of $\alpha$-U. This work shows that isolated point defects cannot be the primary driving force responsible for the significant irradiation induced growth of $\alpha$-U observed experimentally.

## 1. Introduction

Uranium (U) is an actinide element exhibiting delocalized f-electrons that exists in three solid phases: $\alpha$ (face-centered orthorhombic), $\beta$ (tetragonal with a 30 atom unit cell) and $\gamma$ (body-centered cubic) [1]. Below 935 K, U exists in the $\alpha$ phase [2]. Although uranium is alloyed with Mo or Zr in order to stabilize the preferred body-centered cubic phase at lower temperatures, most notably for nuclear fuel applications, the

---

*Corresponding author
Email address:* `bwbeeler@ncsu.edu` (Benjamin Beeler)

$\alpha$ phase persists either in decomposed phase regions (as in the case of U-Mo fuel), or in the low temperature periphery of the fuel slug (as in the case of U-Zr type fuel). Because of its unique crystal structure, $\alpha$-U exhibits anisotropic material properties, for example, thermal expansion [3] and elastic constants [4]. One relevant behavior is the anisotropic irradiation growth of $\alpha$-U [5], which can lead to the tearing along grain boundaries and the formation of crystallographically aligned pores. These porosities are believed to form due to the interaction of lattice defects and stresses induced by irradiation and a temperature gradient, and result in significant volume changes of $\alpha$-U [5, 6]. A full understanding of the relationship between point defects, lattice strains, and the generation of pores, has not been established either experimentally or via computational methods. However, a number of computational studies have been performed into fundamental properties of uranium [7].

Density functional theory (DFT) is an essential part of computational materials science, addressing a variety of problems in materials design and processing on a fundamental level. Several examinations of U via DFT have been performed on its orthorhombic and body-centered cubic (bcc) structures. Taylor [8] used a projector augmented wave (PAW) pseudo-potential to calculate the lattice constants of $\alpha$-U and $\gamma$-U along with the bulk modulus of both phases and the surface energy of a single surface in $\alpha$-U. Xiang, *et al.* [9] also utilized a PAW pseudo-potential to perform an analysis of lattice constants in the $\alpha$ and $\gamma$ phases, as well as an analysis of defects in $\gamma$-U. Beeler, *et al.* calculated the lattice constants and elastic constants of $\alpha$, $\beta$ and $\gamma$-U [10], in addition to the point defect properties in both $\alpha$ and $\gamma$-U [11]. Huang and Wirth [12, 13] calculated intrinsic and extrinsic point defect formation energies and migration barriers in $\alpha$-U. These DFT investigations showed a general, if imperfect, agreement with the experimental bulk moduli, lattice and elastic constants, and vacancy formation energy [1, 14, 15].

Key areas lacking from the DFT-based literature on $\alpha$-U include an analysis of temperature-dependent bulk properties, including thermal expansion and heat capacity, and temperature-dependent defect properties. Extrapolation of 0 K properties to compare to elevated temperature experiments can be ill-advised, particularly for complex crystal structures or for point defects. However, *ab initio* molecular dynamics (AIMD) allows for quantum mechanical-based calculations to be performed at non-zero temperatures. AIMD has been utilized to study a variety of systems including liquid phase diffusion in Al-Si [16], adsorption energy of Fe on TiN surfaces [17], NaCl dissolution in water [18] and finite temperature phonon dispersion curves in bcc Zr and bcc Li [19]. Hood, *et al.* [20] have previously utilized AIMD to study the equation of state of U and the variation in density of states for the liquid phase of U at two unique temperatures. Hood, *et al.* utilized a unique pseudo-potential that was presented in that same manuscript [20]. Soderlind, *et al.* [21] utilized self-consistent *ab initio* lattice dynamics (SCAILD) to study the high temperature stabilization of the $\gamma$-U phase by calculating phonon modes at 1100 K. There have been several investigations of the free energy via the temperature dependent effective potential (TDEP) technique [22, 23, 24, 25, 26], and one recent AIMD investigation into the defect formation energies in $\gamma$-U at high temperatures [27]. Despite numerous investigated into metallic uranium, AIMD has not been deployed to study temperature dependent

properties of $\alpha$-U, such as thermal expansion or defect formation energies.

In this work, AIMD simulations are performed to calculate the equilibrium volume of $\alpha$-U as a function of temperature. Utilizing these equilibrium volumes, the three lattice constants of $\alpha$-U are determined, yielding anisotropic thermal expansion calculations. Additionally, point defect formation energies for interstitials and vacancies are calculated as a function of temperature. The lattice strain from the introduction of these point defects is calculated, providing insight into the fundamental stages of irradiation growth. This is the first AIMD investigation of point defects in $\alpha$-U.

## 2. Computational Details

Systems are investigated using the Vienna *ab initio* Simulation Package (VASP) [28, 29, 30, 31]. The projector augmented wave (PAW) method [32, 33] is utilized within the density functional theory [34, 35] framework. Calculations are performed using the Perdew-Burke-Ernzerhof (PBE) [36, 37] generalized gradient approximation (GGA) density functional implementation for the description of the exchange-correlation. A uranium PAW pseudo-potential with the $6s^2 6p^6 5f^3 6d^1 7s^2$ valence electronic configuration and a core represented by [Xe, 5d, 4f] is utilized. Methfessel and Paxton's smearing method [38] of the first order is used with a width of 0.1 eV to determine the partial occupancies for each wave-function. A Monkhorst-Pack [39] 1x1x1 k-point mesh was utilized for Brillouin zone sampling. Uranium is assumed to be non-magnetic, in accordance with both experiments [40] and previous simulations [10], and as such calculations are non-spin-polarized. The Hubbard U term is not applied to the $f$ electrons, in accordance with previous computational studies that utilized DFT on $\alpha$-U [12, 13, 8, 10]. The precision is set to normal and the energy cutoff is increased to 300 eV. The electronic self-consistent loop exit criterion is set to $10^{-4}$ and the precision for projectors in real space is increased to $-10^{-4}$. A 180 atom supercell (5x3x3 unit cells) is utilized for all simulations. Such a supercell is sufficiently large to preclude defect-defect interactions. Dynamics were carried out in the NpT ensemble with Parinello-Rahman dynamics and a Langevin thermostat to control temperature. The temperature range investigated is from 100 K to 800 K, in increments of 100 K, to span nearly the entire range of stability of the $\alpha$ phase of U. The Langevin friction coefficient for both the atomic and lattice degrees-of-freedom was set to 5 ps$^{-1}$, with a fictitious mass for the lattice degrees of freedom of 500 amu. The timestep is set to 2.0 fs, and the initial structures are equilibrated at the target temperature for 8 ps. The trajectories of the total supercell energy, pressure, and individual lattice vectors are analyzed as a function of timestep to ensure that an equilibrated state has been reached and each of these quantities are oscillating around a given value, with the pressure oscillating around zero. Subsequently, the simulations are further equilibrated for 2000 timesteps (4 ps) for the determination of equilibrium properties. In order to obtain average properties over the *ab initio* molecular dynamics simulation, the energies and lattice constants for the final 1500 timesteps (3 ps) are extracted and averaged. In order to ensure statistical significance of the results, ten unique simulations are performed for each individual simulation setup.

The thermal expansion is calculated both for individual lattice constants, and as a volume averaged value, via equation 1:

$$\alpha = \frac{L - L_0}{L_0} \tag{1}$$

where $\alpha$ is the thermal expansion, and L is the length of the individual lattice constant or averaged lattice constant at a given temperature, and $L_0$ is the reference length at a given temperature. The formation energy of point defects is calculated via equation 2:

$$E_f = E^* - \frac{n \pm 1}{n} \times E_0 \tag{2}$$

where $E^*$ is the energy of a system with a defect (with n $\pm 1$ atoms), $n$ is the number of atoms in the defect-free system and $E_0$ is the energy of a defect-free system with $n$ atoms. Equation 2 utilizes $(n + 1)$ for interstitials and $(n - 1)$ for vacancies. The molar heat capacity is determined from equation 3:

$$C_P = \left( \frac{\delta H}{\delta T} \right)_P \tag{3}$$

where H is the enthalpy (potential plus kinetic energy), T is the temperature, and it is emphasized that this is determined for a constant pressure, which in these simulations is zero pressure. The total heat capacity is a sum of the lattice (Eq. 3) and the electronic components of the heat capacity. The electronic heat capacity coefficient ($\gamma_e$, where the electronic heat capacity is $\gamma_e \times$T) has been experimentally reported to be 10.12 mJ/mol-K$^2$ [41, 42] , and this value is utilized here to determine the total heat capacity as a function of temperature.

## 3. Results

### 3.1. Equilibrium properties of $\alpha$-U

The equilibrium lattice constants at room temperature were calculated to be: $a = 2.78$ Å, $b = 5.91$ Å, and $c = 4.93$ Å. These results compare very favorably to the experimental literature ($a = 2.85$Å, $b = 5.86$Å, and $c = 4.96$ Å[43]), with the largest deviation observed for the $a$ lattice constant at a magnitude of approximately 2.5%. Some deviation is not unexpected, as it has been shown that DFT calculations do not always exactly match the experimental findings, particularly for the lattice constant. However, these results are in accordance with previously computational investigations of $\alpha$-U performed at 0 K, when thermal expansion is taken into account [12, 10].

The normalized lattice constants as a function of temperature are shown in Fig. 1. Each lattice constant is normalized to its determined value at 100 K, which is the lowest temperature analyzed. Thermal expansion occurs in both the $a$ and $c$ directions, while thermal contraction occurs in the $b$ direction, as has been previously experimentally observed [44]. Average values for linear thermal expansion coefficients of $\alpha$-U for the $a$, $b$, and $c$ crystallographic directions were experimentally determined to be $26.5 \times 10^{-6}$ K$^{-1}$,

-2.4×10$^{-6}$ K$^{-1}$, and 23.9×10$^{-6}$ K$^{-1}$, respectively, over the temperature range of 298-598 K [44, 3]. The data in Fig. 2 utilizes 300 K as the reference point for both the AIMD data and the experimental data, and as such, the change in length at 300 K is zero. It can be observed that the AIMD predicted thermal expansion in the $a$ direction is significantly greater than that determined from experiment. Similarly, the amount of contraction in the $b$ direction predicted from AIMD is significantly greater than that observed in experiments. However, the $c$ direction exactly matches the linear thermal expansion determined from experiments. Qualitatively, all of the behaviors are identical, with the $a$ and $b$ directions expressing a more extreme expansion/contraction behavior. The source of the deviations from experiment are currently unknown. It should be noted that significant scatter exists in the experimental datasets utilized to generate the averages presented for comparison in Fig. 2, and additional experimental investigations are warranted in order to confirm previous findings.
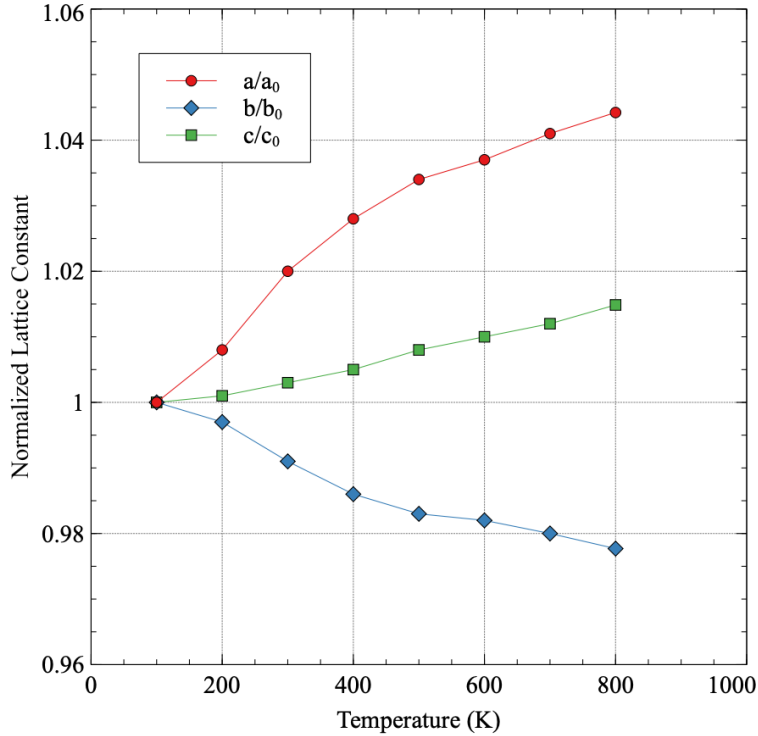


Figure 1: The normalized lattice constants as a function of temperature for $\alpha$-U. Each lattice constant is normalized to its value at 100 K.
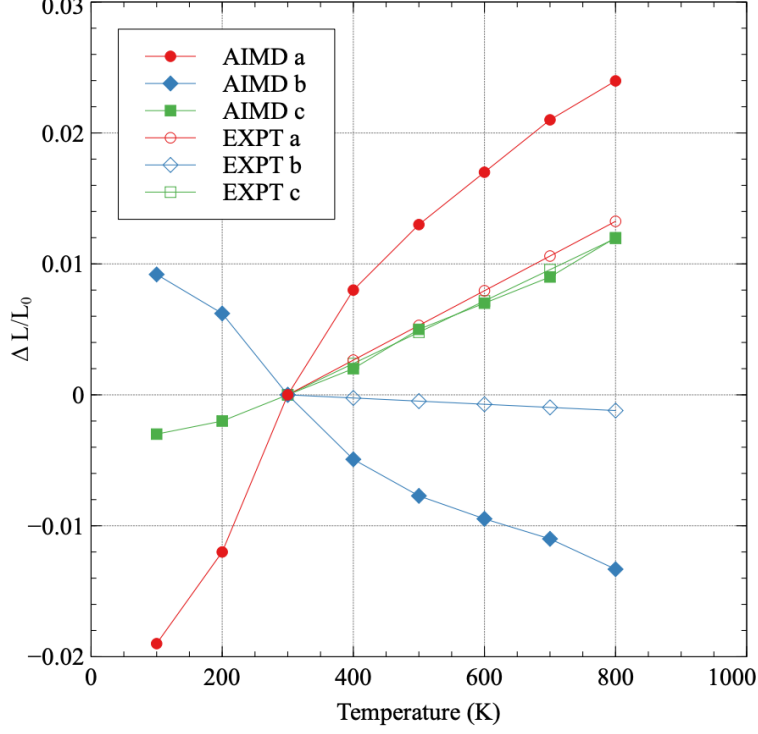
Figure 2: The linear thermal expansion coefficient for each lattice constant in $\alpha$-U. Thermal expansion is normalized to 300 K, which is the lowest temperature in the experimental data [44, 3].

The volume-averaged thermal expansion is calculated and compared to a different set of experimental results from Touloukian [45] in Fig. 3. Interestingly, the data from AIMD nearly exactly matches the experimental results for volumetric-averaged thermal expansion, with only slight deviations presenting above 600 K. Thus, despite the differences in the individual components of thermal expansion in $\alpha$-U, which are somewhat substantial, the cumulative effect on total volume expansion reproduces the experimental observations.
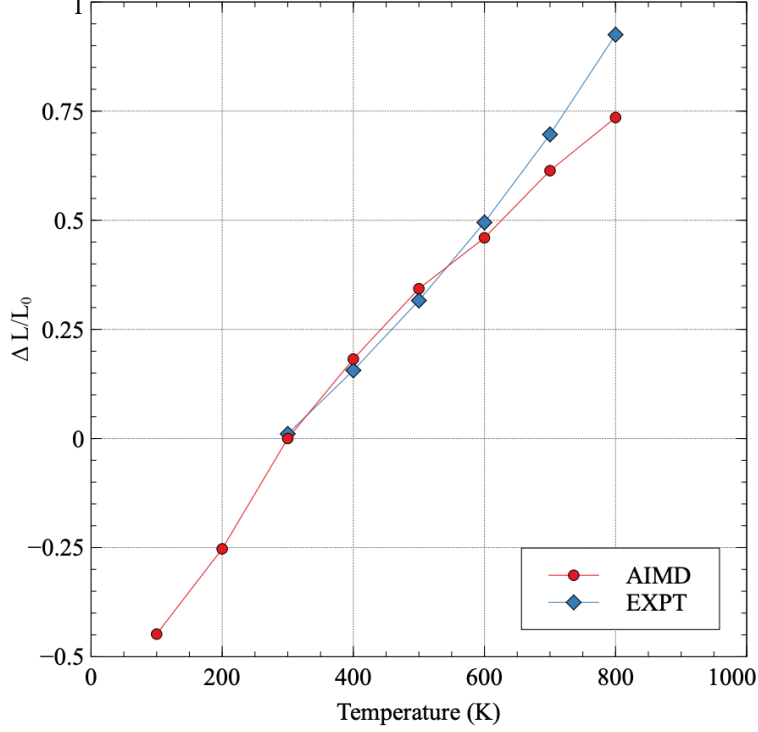
Figure 3: Volume-averaged linear thermal expansion in $\alpha$-U. Thermal expansion is taken with respect to 300 K and compared to experimental results [45].

The total constant pressure heat capacity is determined from a summation of equation 3 and the electronic heat capacity contribution as determined by experiments, and is plotted in Fig. 4. Data point are shown at intermediate temperatures, as the formalism in equation 3 assumes effectively a constant value of $C_p$ over the temperature range. Thus, utilizing data points at 100 K and 200 K, for example, yields a value of $C_p$ at 150 K in this work. Experimental data is only reported for room temperature and upwards, and the agreement with the AIMD is generally excellent. The maximum deviation is observed at 750 K, where the AIMD results under-predict the magnitude of $C_p$ by approximately 11%. At lower temperatures, the deviation can be less than 5%. Thus, while the magnitude of the heat capacity is generally the same, it appears that the experimentally observed heat capacity is more sensitive to temperature, showing a total change from 250-750 K of 17 J/mol-K, while AIMD only predicts at increase of 11 J/mol-K over this temperature range.
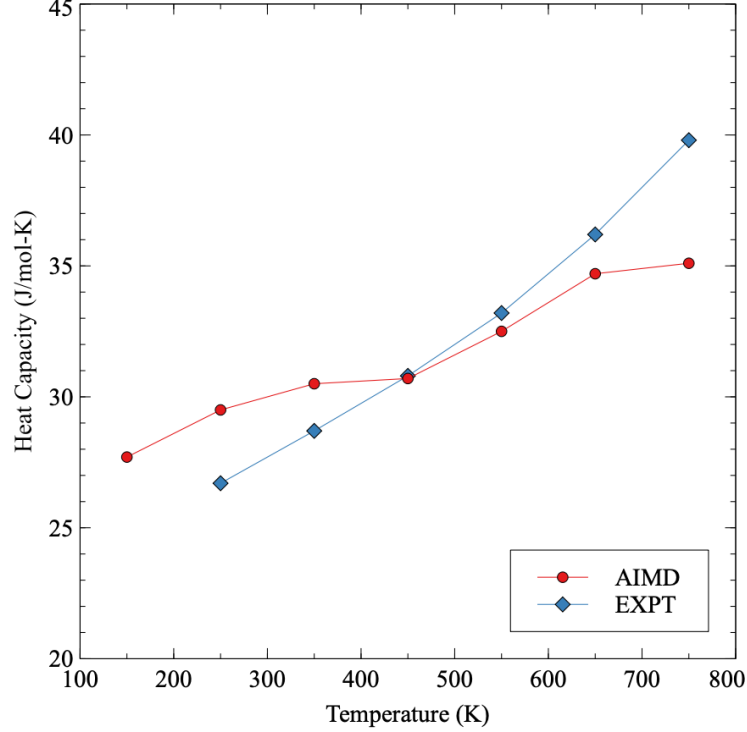
Figure 4: The constant pressure heat capacity of $\alpha$-U from 100 K to 800 K. Results from this work are compared to experimental results from Konings [46].

## 3.2. Point defects in $\alpha$-U

The point defect formation energy of interstitials and vacancies in $\alpha$-U is shown in Fig. 5. The defect formation energy for both types of defects tends to slightly decrease with increasing temperature until approximately 400 K. Above 400 K, an increase in the defect formation energy with increasing temperature is observed. The relative magnitudes of the defect formation energies with respect to one another are near constant across the entire temperature range investigated, with the average interstitial formation energy (3.4 eV) about 2.3 times the average vacancy formation energy (1.46 eV). Error bars shown in Fig. 5 are twice the standard error, where the standard error for formation energies is defined as

$$SE^2 = \frac{\sigma_{bulk}}{\sqrt{N}} + \frac{\sigma_{def}}{\sqrt{N}} \tag{4}$$

where $\sigma_{bulk/defect}$ is the standard deviation of the dataset utilized for determining the average energies of either the defect-free or the defected system, and $N$ is the sample size, which is ten simulations. The standard error in the data set tends to increase with increasing temperature, as would be expected. The results from the lower temperature regime can be compared to previous results from 0 K DFT calculation. At 100 K, the interstitial formation energy is found to be 3.81 eV, and the vacancy formation energy is found to be 1.69 eV. These results compare favorably to previous 0 K DFT results [12], which showed a vacancy formation energy of 1.69 eV (an exact match), and interstitial formation energy of 4.42 eV. That the

8

interstitial formation energy from this work is lower is not unsurprising, as the effect of temperature can yield additional relaxation pathways or defect reorientation that is not strictly achievable through calculations at 0 K. However, the magnitude of the relaxation cannot be reasonably estimated from 0 K, and thus requires these high temperature calculations to determine true defect behavior at non-zero temperature. This data can be utilized to conduct higher length scale simulations which attempt to describe defect formation and mobility and those which include an estimation of the equilibrium concentrations of defects.
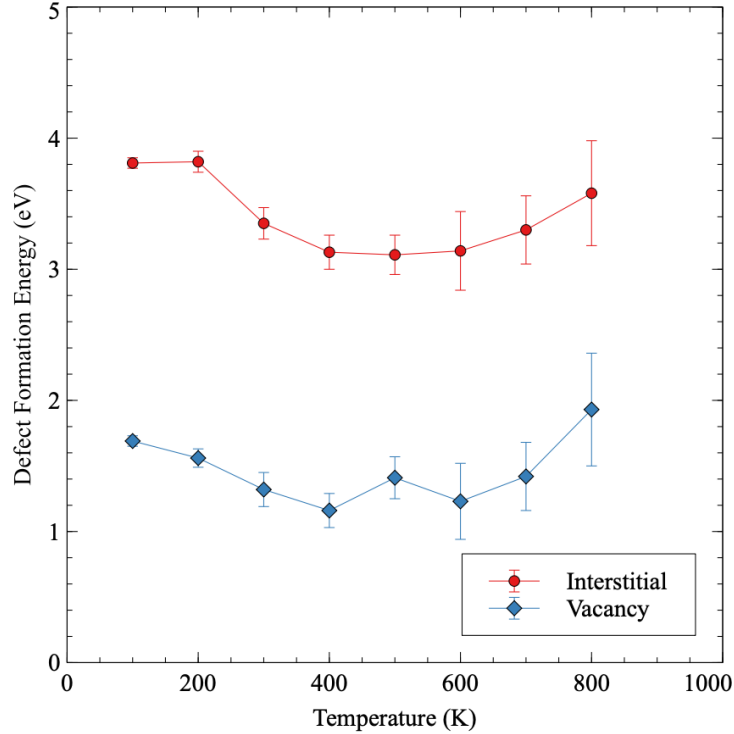


Figure 5: The formation energy of an interstitial and a vacancy in $\alpha$-U as a function of temperature.

The introduction of a defect and relaxation in an NpT ensemble allows for the analysis of volume changes due to individual point defects. These volume changes are reported as a function of temperature in Fig. 6. For interstitials, there clearly exist two distinct regimes in the defect-induced strain environment, with 400 K serving as the demarcation temperature. Below 400 K, strain is relatively large and positive (lattice expansion) in the $a$ direction, and relatively large and negative (lattice compression) for the $b$ direction. The magnitudes of those strains decrease with increasing temperature up to 400 K, above which they maintain a relatively fixed value, with some statistical fluctuation. It is unknown whether the deviation at 600 K is due to some distinct behavioral changes, or is simply the result of thermal noise. However, data points at 600 K remains within the standard error of the general trend (standard error not shown here for readability of figures), which implies that it is unlikely to indicate a change in behavior. The $c$ lattice constant exhibits very slight positive strain across the entire temperature range, with no obvious changes in behavior. For vacancies, the general magnitude of the strain is significantly less than that observed for interstitials, with the maximum

strain of 0.5% observed at 800 K for the $b$ lattice constant. While it is more difficult to discern trends in the vacancy strain as a function of temperature, several pieces of information can be readily extracted. The $c$ lattice constant displays no observed strain from vacancies at any temperature. For the $a$ and $b$ lattice constants, opposite trends present themselves above 400 K, in that the $a$ lattice constant strain increases with increasing temperature and the $b$ lattice constant strain decreases with increasing temperature. In a general sense, the strain behavior of defects is as expected, in that interstitials yield a lattice expansion, while vacancies produce lattice contraction. However, the manner in which those volumetric averages are produced is quite complex, and is significantly temperature dependent.
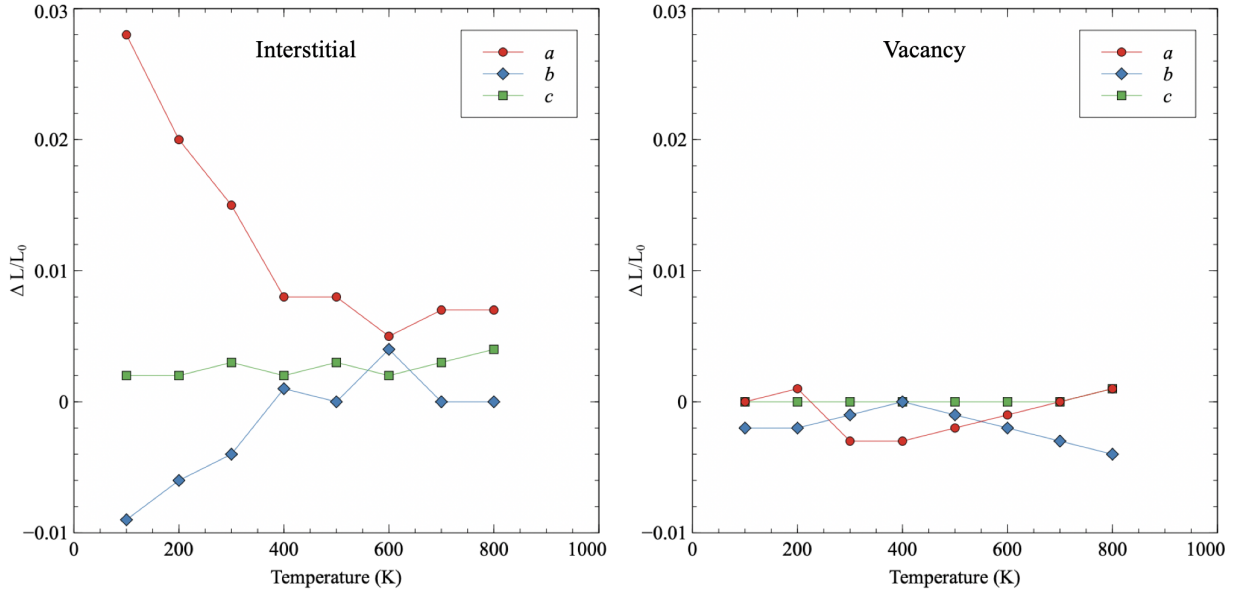


Figure 6: The lattice strain induced from an interstitial or vacancy in $\alpha$-U as a function of temperature.

## 4. Discussion

This work indicates a number of lattice and volume effects that are strongly dependent upon the temperature of the system. Excepting the heat capacity, all of these calculated properties seem to indicate two regions of behavior, one below 400 K and one above 400 K. Also, it should be re-emphasized that the heat capacity utilized an experimental data point for the determination of the electronic heat capacity. Thus, from the purely computationally obtained data, there are differences in lattice constant, defect-induced lattice strain, and defect formation energy, in these two temperature regimes. To briefly summarize, thermal expansion expansion/contraction in the $a/b$ direction occurs rapidly from 100 K up to 400 K, after which a more linear and gradual change in the lattice constant takes place. Defect formation energies decrease in magnitude up to 400 K, above which they tend to slightly increase. Defect lattice strains for interstitials

decrease/increase in the $a/b$ direction up to 400 K, above which they maintain essentially the same magnitude. A similar trend in defect lattice strains for vacancies is present, but the magnitude is significantly less and potentially swamped by thermal fluctuations, and thus the statistical certainty of the finding is reduced.

In an attempt to identify underlying changes in the atomic and electronic structure as a function of temperature, two additional analyses were performed. The first was a coordination analysis, in which the radial distribution function (rdf) was constructed for a snapshot of the equilibrated $\alpha$-U structure at 200 K, 400 K, and 700 K. If a modification in the bond lengths is occurring that can yield differences in structure, such a modification would present itself as peak shifts in the rdf. This coordination analysis yielded no discernible trends, and the general bond length and peak broadening confirms what is observed in Fig. 1 and Fig. 2 outlining thermal expansion. The second analysis involved the electronic density of states (DOS). If the character of valence electrons participating in the bonding are changing as a function of temperature, the electronic DOS would identify such changes. The electronic DOS was calculated, and only minimal variation in the electronic structure was observed as a function of temperature. There was no indication that two regions of electronic structure behavior exist for the $\alpha$ phase. Due to the lack of identifiable structure variation as a function of temperature, these results are not displayed here, as the DOS and rdf can be obtained from the literature [10, 20]. The underlying cause of the apparent two-region behavior is unclear, and warrants further computational investigation, in addition to experimental studies on high-purity uranium to either confirm or refute the findings in this work.

This work has identified that individual point defect can produce somewhat significant lattice strain, but it is unknown if such point defects could be responsible for experimentally observed macroscopic shape change. Comparison of the calculated direction of the defect-induced strains to the experimental literature on irradiation growth provides contradictory information. Paine and Kittel [6] and Loomis and Gerber [47] both investigated dimensional change of single crystal uranium under irradiation. Their findings were in general agreement with one another, and showed a contraction of the bulk crystal in the $a$ direction, an expansion in the $b$ direction, and no change in the $c$ direction. While the AIMD results of point defect-induced strains presented here agree with the lack of dimensional change in the $c$ direction, exactly the opposite behavior is observed in Fig. 6 for the $a$ and $b$ directions. This work showed that interstitials are the dominant strain inducers, producing expansion in the $a$ direction and contraction in the $b$ direction. Due to the relatively large induced strains from interstitials, it is expected that these types of point defects would display strongly anisotropic diffusion. Given that isolated point defects lead to the opposite trends from those observed experimentally, it is possible that defect clusters or defect loops display different strain behaviors than individual point defects, and are the features responsible for irradiation growth in $\alpha$-U. Such research is beyond the scope of AIMD, which is currently sufficiently computationally expensive to exclude the possibility of analysis of extended defects. Thus, classical molecular dynamics simulations can be performed, and validated against the work presented here. Ideally, in addition to further computational studies, the experimental results from over sixty years ago should be reproduced and modern characterization

methods applied to extract fundamental defect populations, densities, and orientations.

## 5. Conclusions

In this study, AIMD simulations were performed to calculate temperature-dependent properties of the $\alpha$ phase of U from 100 K to 800 K. The thermal expansion of each individual lattice constant was analyzed and compared to the experimental literature. Although the general direction of thermal expansion corresponded to the experimental findings (positive in $a$ and $c$, negative in $b$), the magnitudes of coefficient of thermal expansion for the $a$ and $b$ directions was greater than that observed experimentally. However, the volumetric expansion corresponded nearly exactly to the experimental findings in the literature. The heat capacity was calculated as a function of temperature and showed a general agreement with experimental results, although the computationally determined heat capacity was slightly less sensitive to temperature. Variation in point defect formation energies was determined, with an average interstitial formation energy of 3.40 eV, and an average vacancy formation energy of 1.46 eV, over the entire temperature range. Lattice strains resulting from point defects were determined, showing that interstitials induce significantly more strain than vacancies, and the nature of that strain is highly dependent on the individual lattice directions, where the $a$ direction expands and the $b$ contracts due to the introduction of an interstitial. Finally, all of these results seem to indicate a two-region behavior, with the transition at 400 K. The thermal expansion expansion/contraction in the $a/b$ direction occurs rapidly from 100 K up to 400 K, after which a more linear and gradual change in the lattice constant takes place. Defect formation energies decrease in magnitude up to 400 K, above which they tend to slightly increase. Defect lattice strains for interstitials decrease/increase in the $a/b$ direction up to 400 K, above which they maintain essentially the same magnitude. Coordination and electronic structure investigations provided no insight into the possible cause of this potential transition in behavior.

This work has shown that isolated point defects cannot be the primary driving force responsible for the significant irradiation induced growth of $\alpha$-U observed experimentally. This work can be utilized as the basis for mesoscale simulations that take into account defect populations, defect diffusion, and defect strain behaviors. It is emphasized that additional computational work utilizing classical molecular dynamics on extended defects should be performed, in addition to experimental irradiation and characterization, to further elucidate the underlying phenomena governing the interactions of point defects with the $\alpha$-U crystal structure.

## 6. Acknowledgement

## References

[1] C.-S. Yoo, H. Cyun, P. Soderlind, Phase diagram of uranium at high pressures and temperatures, Phys. Rev. B 57 (1998) 10359.

[2] P. Soderlind, Theory of the crystal structures of cerium and the light actinides, Adv. in Phys. 47 (1998) 959.

[3] L. Lloyd, C. Barrett, Thermal expansion of alpha uranium,, J. Nucl. Mater. 18 (1966) 55.

[4] E. Fisher, H. McSkimin, Adiabatic elastic moduli of single crystal alpha uranium, J. Appl. Phys. 29 (1958) 1473.

[5] R. Leggett, T. Bierlein, B. Mastel, Irradiation behavior of high purity uranium, Tech. Rep. HW-79559, Hanford Laboratories (1963).

[6] S. Paine, J. Kittel, Preliminary analysis of fission-induced dimensional changes in single crystals of uranium, Tech. Rep. ANL-5676, Argonne National Laboratory (1958).

[7] A. Jokisaari, Irradiation-induced internal stresses in polycrystalline alpha-uranium: a mesoscale mechanical approach, Comp. Mat. Sci. 176 (2020) 109545.

[8] C. Taylor, Evaluation of first-principles techniques for obtaining materials parameters of alpha uranium and the (001) alpha uranium surface, Phys. Rev. B 77 (2008) 094119.

[9] S. Xiang, H. Huang, L. Hsiung, Quantum mechanical calculations of uranium phases and niobium defects in gamma-uranium, J. Nucl. Mater. 375 (2008) 113.

[10] B. Beeler, C. Deo, M. Baskes, M. Okuniewski, First principles calculations of the structure and elastic constants of alpha, beta and gamma uranium, J. Nucl. Mater. 433 (2013) 143.

[11] B. Beeler, B. Good, S. Rashkeev, C. Deo, M. Baskes, M. Okuniewski, First principles calculations for defects in U, J. Phys.: Cond. Mat. 22 (2010) 505703.

[12] G.-Y. Huang, B. Wirth, First-principles study of diffusion of interstitial and vacancy in alpha U-Zr, J. Phys.: Cond. Mat. 23 (2011) 205402.

[13] G.-Y. Huang, B. Wirth, First-principles study of bubble nucleation and growth behaviors in alpha u-zr, J. Phys.: Cond. Mat. 24 (2012) 415404.

[14] C. Barrett, H. Mueller, R. Hitterman, Crystal structure variations in alpha uranium at low temperatures, Phys. Rev. 129 (1963) 625.

[15] H. Matter, J. Winter, W. Triftshauser, Investigation of vacancy formation and phase transformations in uranium by positron annihilation, J. Nucl. Mater. 88 (1980) 273.

[16] V. Manga, D. Poirier, Ab initio molecular dynamics simulation of self-diffusion in al–si binary melts, Modelling Simul. Mater. Sci. Eng. 26 (2018) 065006.

[17] C. Wang, Y. Dai, H. Gao, X. Ruan, J. Wang, B. Sun, Ab initio molecular dynamics study of fe adsorption on tin (001) surface, Mat. Trans. 51 (2010) 2005.

[18] J. Timko, D. Bucher, S. Kuyucak, Dissociation of nacl in water from ab initio molecular dynamics simulations, J. Chem. Phys. 132 (2010) 114510.

[19] O. Hellman, I. A. Abrikosov, S. I. Simak, Lattice dynamics of anharmonic solids from first principles, Phys. Rev. B 84 (2011) 180301(R).

[20] R. Hood, L. Yang, J. Moriarty, Quantum molecular dynamics simulations of uranium at high pressure and temperature, Phys. Rev. B 78 (2008) 024116.

[21] P. Soderling, B. Grabowski, L. Yang, A. Landa, T. Bjorkman, P. Souvatis, O. Eriksson, High-temperature phonon stabilization of ! -uranium from relativistic first-principles theory, Phys. Rev. B 85 (2012) 060301.

[22] O. Hellman, P. Steneteg, I. Abrikosov, S. Simak, Temperature dependent effective potential method for accurate free energy calculations of solids, Phys. Rev. B 87 (2013) 104111.

[23] V. Ladygin, P. Korotaev, A. Yanilkin, A. Shapeev, Lattice dynamics simulation using machine learning interatomic potentials, Comp. Mat. Sci. 172 (2020) 109333.

[24] I. Kruglov, A. Yanilkin, A. Oganov, P. Korotaev, Phase diagram of uranium from ab initio calculations and machine learning, Phys. Rev. B 100 (2019) 174104.

[25] J. Bouchet, F. Bottin, High-temperature and high-pressure phase transitions in uranium, Phys. Rev. B 95 (2017) 054113.

[26] A. Castellano, F. Bottin, B. Dorado, J. Bouchet, Thermodynamic stabilization of $\gamma$-u-mo alloys: Effect of mo content and temperature, Phys. Rev. B 101 (2020) 184111.

[27] B. Beeler, D. Andersson, C. Jiang, Y. Zhang, Ab initio molecular dynamics investigation of point defects in gamma-u, J. Nucl. Mater. 545 (2020) 152415.

[28] G. Kresse, J. Hafner, Ab initio molecular dynamics for liquid metals, Phys. Rev. B 47 (1993) 558.

[29] G. Kresse, J. Hafner, Ab initio molecular-dynamics simulation of the liquid-metal-amorphous-semiconductor transition in germanium, Phys. Rev. B 49 (1994) 14251.

[30] G. Kresse, J. Furthmuller, Efficiency of ab-initio total energy calculations for metals and semiconductors using a plane-wave basis set, Comput. Mat. Sci. 6 (1996) 15.

[31] G. Kresse, J. Furthmuller, Efficient iterative schemes for ab initio total-energy calculations using a plane-wave basis set, Phys. Rev. B 54 (1996) 11169.

[32] P. Blochl, Projector augmented-wave method, Phys. Rev. B 50 (1994) 17953.

[33] G. Kresse, D. Joubert, From ultrasoft pseudopotentials to the projector augmented-wave method, Phys. Rev. B 59 (1999) 1758.

[34] P. Hohenberg, W. Kohn, Inhomogeneous electron gas, Phys. Rev. 136 (1964) B864.

[35] W. Kohn, L. Sham, Self-consistent equations including exchange and correlation effects, Phys. Rev. 140 (1965) A1133.

[36] J. Perdew, K. Burke, M. Ernzerhof, Generalized gradient approximation made simple, Phys. Rev. Lett. 77 (1996) 3865.

[37] J. Perdew, K. Burke, M. Ernzerhof, Erratum: Generalized gradient approximation made simple, Phys. Rev. Lett. 78 (1997) 1396.

[38] M. Methfessel, A. Paxton, High-precision sampling for brillouin-zone integration in metals, Phys. Rev. B 40 (1989) 3616.

[39] H. Monkhorst, J. Pack, Special points for brillouin-zone integrations, Phys. Rev. B 13 (1976) 5188.

[40] D. Lide, Handbook of Chemistry and Physics: A Ready-Reference Book Chemical and Physical Data, CRC-Press, 2000.

[41] D. Marchidan, M. Ciopec, Enthalpy of uranium to 1500 k by drop calorimetry, J. Chem. Thermo. 8 (1976) 691.

[42] L. Schachinger, I. Lamprecht, Heat capacity of uranium metal at low temperatures. a reminiscence., Thermoc. Acta 151 (1989) 203.

[43] A. Lawson, C. Olsen, J. Richardson, M. Mueller, G. Lander, Structure of beta-uranium, Acta Crys. B44 (1988) 89.

[44] I. Grenthe, J. Drożdżyński, T. Fujino, E. Buck, T. Albrecht-Schmitt, S. Wolf, Uranium, in: The Chemistry of the Actinide and Transactinide Elements, Springer, Dordrecht, The Netherlands, 2010.

[45] Y. Touloukian, R. Kirby, R. Taylor, P. Desai, Thermophysical Properties of Matter - Thermal Expansion: Metallic elements and alloys, Vol. 12, IFI/Plenu,, 1975.

[46] R. Konings, O. Benes, The thermodynamic properties of the f-elements and their compounds. i. the lanthanide and actinide metals, Journal of Physical and Chemical Reference Data 39 (2010) 043102.

[47] B. Loomis, S. Gerber, Length and electrical resistivity changes of neutron irradiated uranium, Phil. Mag. 18 (1968) 539.